

Applications of the source-frequency phase-referencing technique for ngEHT observations

Wu Jiang^{1,2,*}, Guang-Yao Zhao^{3,*}, Zhi-Qiang Shen^{1,2}, María Rioja^{4,5,6}, Richard Dodson⁴, Ilje Cho³, Shan-Shan Zhao^{1,2}, Marshall Eubanks⁷ and Ru-Sen Lu^{1,2,8}

¹ Shanghai Astronomical Observatory, Chinese Academy of Sciences, Shanghai 200030, China.

² Key Laboratory of Radio Astronomy, Chinese Academy of Sciences, Nanjing 210008, China.

³ Instituto de Astrofísica de Andalucía-CSIC, Glorieta de la Astronomía s/n, 18008 Granada, Spain.

⁴ ICRAR, M468, The University of Western Australia, 35 Stirling Hwy, Crawley, Western Australia, 6009, Australia

⁵ CSIRO Astronomy and Space Science, PO Box 1130, Bentley WA 6102, Australia

⁶ Observatorio Astronómico Nacional (IGN), Alfonso XII, 3 y 5, 28014 Madrid, Spain

⁷ Space Initiatives Inc, Newport, VA 24128, USA

⁸ Max-Planck-Institut für Radioastronomie, Auf dem Hügel 69, D-53121 Bonn, Germany.

* Correspondence: jiangwu@shao.ac.cn; gyzhao@iaa.es

Abstract: The source-frequency phase-referencing (SFPR) technique has been demonstrated to have great advantages for mm-VLBI observations. By implementing simultaneous multi-frequency receiving systems on the next generation Event Horizon Telescope (ngEHT) antennas, it is feasible to carry out a frequency phase transfer (FPT) which could calibrate the non-dispersive propagation errors and significantly increase the phase coherence in the visibility data. Such increase offers an efficient approach for weak source or structure detection. SFPR also makes it possible for high precision astrometry, including the core-shift measurements up to sub-mm wavelengths for Sgr A* and M 87* etc. We also briefly discuss the technical and scheduling considerations for future SFPR observations with the ngEHT.

Keywords: Black hole; VLBI; ngEHT; Astrometry; SFPR

1. Introduction

The Very Long Baseline Interferometry (VLBI) technology can achieve the highest spatial angular resolution by linking intercontinental telescopes to form a virtual telescope, whose aperture size is equal to the longest baseline in the array. However, the wavefront arriving at each telescope suffers from various phase fluctuations when propagating through the atmosphere. This is even more severe at the millimeter and sub-millimeter (sub-mm) wavelengths as the phase dispersion is in proportion to the observing frequency. A novel technique called frequency phase transfer (FPT) [?] or source-frequency phase-referencing (SFPR) [2] is proposed to mitigate the fast phase fluctuations at the shorter wavelengths, by referring to the phases at the longer wavelength observed close in time. The phases could be purified by two step calibrations. The first step is the FPT calibration, where the non-dispersive phase errors, such as the tropospheric phase errors and the geometric antenna position errors, are removed. Furthermore, the unmodeled ionospheric delay and the instrumental phase offsets between the two wavelengths can be further eliminated by observations of a nearby calibrator. After the SFPR calibrations, the remaining phases just reflect the true high frequency visibilities and the frequency-dependent shift in the positions, e.g., the frequency-dependent location of the jet cores (core-shift) [3]. SFPR could also help to reliably align the molecular line emission seen at different frequency bands (e.g., [4]). It is of great advantages in probing weak sources and high precision astrometric measuring for the (sub-)mm-VLBI.

The capability of simultaneously receiving at four frequency bands (K/Q/W/D) makes the Korea VLBI Network (KVN) a unique prototype and instrument for the FPT/SFPR observations [5,6]. The capability of fast-switching among receivers at the Very Long Baseline Array (VLBA)



Citation: Jiang, W. et al. Applications of the source-frequency phase-referencing technique for ngEHT observations. *Preprints* 2022, 1, 0. <https://doi.org/>

Publisher's Note: MDPI stays neutral with regard to jurisdictional claims in published maps and institutional affiliations.

Copyright: © 2022 by the authors. Licensee MDPI, Basel, Switzerland. This article is an open access article distributed under the terms and conditions of the Creative Commons Attribution (CC BY) license (<https://creativecommons.org/licenses/by/4.0/>).

also makes it possible to carry out FPT/SFPR observations up to the 3 mm band [2,7], although the switching cycle time introduces coherence losses [see Fig. 6 in 8].

- ngEHT and the necessary of SFPR

Based on the success of capturing the first images of two nearby supermassive black holes with the original Event Horizon Telescope (EHT), one at the center of the distant Messier 87 galaxy (M87*) [9] and the other at our Milky Way galaxy center (Sgr A*) [10], the next generation Event Horizon Telescope (ngEHT) will expand the existing array (new sites) [11] and upgrade the technological deployments (receiving capabilities) significantly [12]. It aims to sharpen our view of the black holes and address fundamental questions about the accretion and jet launching process, together with more black hole shadows captured and even making black hole "movies".

Although the sensitivity of ngEHT would be greatly improved with an ultra-wide bandwidth, the baseline sensitivity will still be limited due to the short coherent integration time at sub-mm wavelengths (a typical coherence time is ~ 10 seconds at 230 GHz [13,14] and even shorter at 345 GHz) and the small dish size of most antennas. SFPR can overcome the coherence time limitation at sub-mm wavelengths. As demonstrated in a separate technical paper of this special issue, the coherence time of the high frequency by referring to the low frequency band could be increased more than 100 folds and extended to hour(s) in the simulations. See Rioja et al. in the same issue for more details. The detection threshold relies on the lower frequency rather than the higher one. Using a typical value of 10-15 sec at 85 GHz, the flux density threshold for targets would become one magnitude lower (~ 10 mJy) and the number of targets would be hundreds under the array sensitivity. We have estimated the SFPR errors that would be introduced when referencing the 255 or 340 GHz data to 85 GHz, with an angular separation of 10° between sources. With simultaneous multi-frequency observations and intra-source switching times between zero and 10 minutes, the astrometric precision is about $3 \mu\text{as}$ and dominated by the static ionospheric residuals. These would make ngEHT more powerful for both astrophysical and astrometric applications.

2. Scientific applications

2.1. Sgr A* and M 87*

Sgr A* and M87* are the prime targets for demonstrating the application of SFPR to observational studies of black holes and jets. SFPR can help reduce the phase error budgets from the atmosphere and instruments, while increasing the coherence time, and thus improve the dynamical range of imaging. Furthermore, SFPR will provide precise measurements to understand the event-horizon-scale structure adjacent to the supermassive black holes.

- Possible core-shift detection of Sgr A*

The mm/sub-mm radio emission from Sgr A* can be produced by two generic models: an accretion flow itself [15,16] and/or an outflow [17]. To discriminate the dominant emission models of Sgr A*, the core shift [e.g., 18,19] can be used without resolving its structure. As for the jet model, based on GRMHD simulations, Mościbrodzka *et al.* [20] suggested the core shift of $\sim 130 \mu\text{as}$ at 22-43 GHz and $\sim 60 \mu\text{as}$ at 86-230 GHz. In a recent study by Fraga-Encinas *et al.* (in prep.), the core shift of Sgr A* is predicted from both accretion disk and jet model with different inclination angles. According to their results, a clear difference in core shift between the two scenarios is shown. Especially at small inclination angle, as has been suggested in recent studies [21–23], the expected core shift at 22-43 GHz is $\lesssim 10 \mu\text{as}$ in accretion disk model while $\gtrsim 100 \mu\text{as}$ in jet model. Our preliminary core shift measurements with the Korean VLBI Network (KVN) and the Very Long Baseline Array (VLBA) at the same frequencies show $\sim 100 \mu\text{as}$ (I. Cho *et al.* in prep). However the robustness has been relatively less due to large astrometric uncertainties which are

mainly originated from 1) the large beam size (for KVN) and 2) the frequency switching mode (for VLBA). Each difficulty can be perfectly overcome through the ngEHT with the dual/triple band receiving capability.

- Connecting the jet and the Black hole for M87*

The EHT 2017 image of M87* has revealed the shadow of the central SMBH [9]. The EHT observations, however, were unable to reliably detect and image the inner jet, likely due to sensitivity limitations and the lack of short baselines in the UV-coverage. At longer wavelengths, we see a well-collimated jet but the emission is optically-thick and we are only able to see the $\tau=1$ surface and the downstream optically-thin jet[24]. Furthermore, the resolution at longer wavelengths are not enough to resolve the shadow[25]. It remains uncertain how exactly the SMBH and the jet are connected. The ngEHT will improve the dynamic range of the 1.3 mm images which could enable the detection of the extended jet emission. However, it could be still challenging due to the steep spectrum of the jet. SFPR covering 86-345 GHz bands offers an alternative way to reliably determine the relative location of the SMBH we see at 1.3 mm and the jet core at longer wavelengths. This is critical in understanding how black holes launch powerful, collimated jets[e.g. 26].

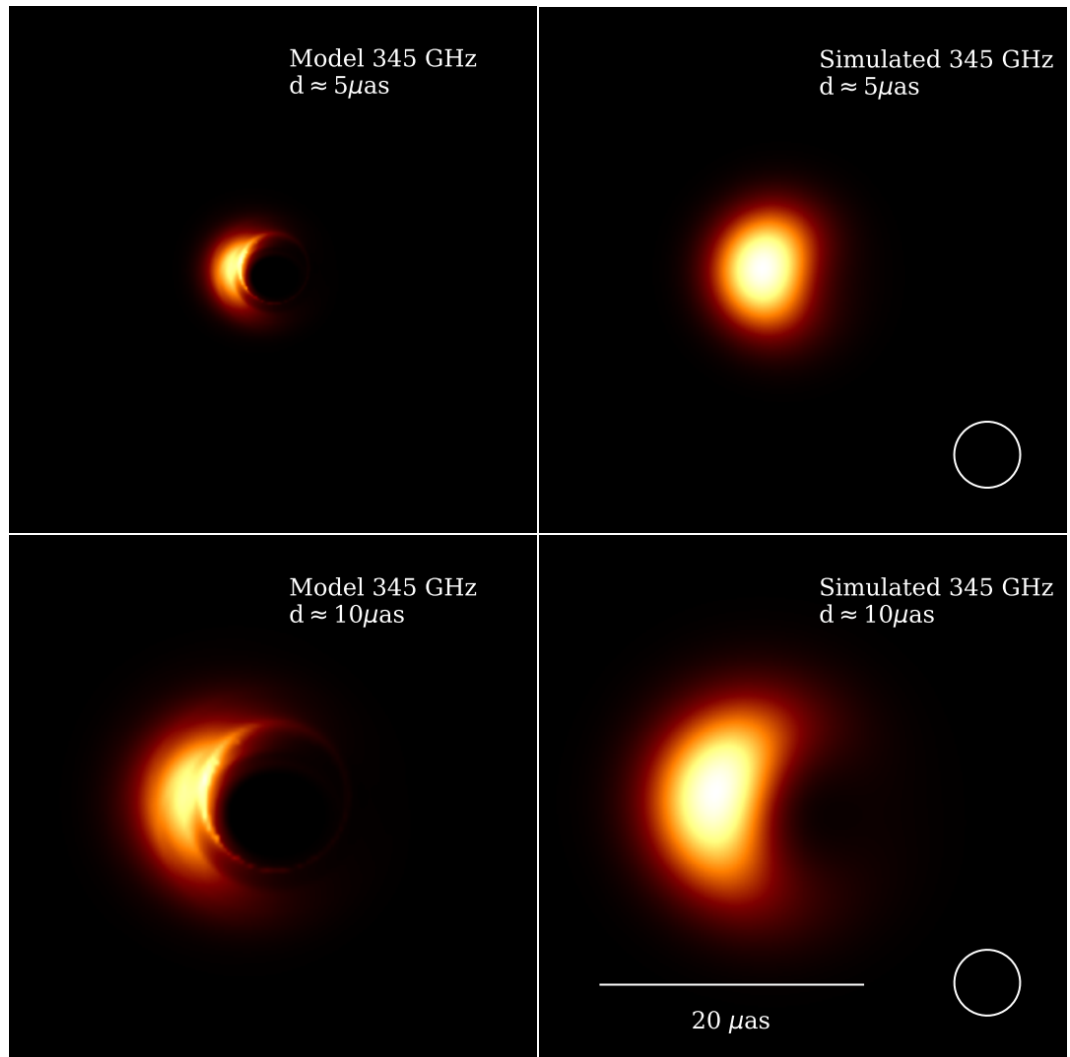


Figure 1. Model images of M84 with two different black hole masses. The images (right column) are reconstructed based on simulated ngEHT observations at 345 GHz. The empty white ring at the right bottom corner of the right panel plots is the synthesized beam of ngEHT at 345 GHz.

2.2. Detection of weak sources and structures

- Toward more supermassive black hole shadows

With the increased coherent integration time, black holes whose radio emissions are weak but shadow sizes are relatively large can be detected by ngEHT. According to the prediction of a semi-analytic spectral energy distribution model [27], there should be a dozen of additional sources with their horizon-scale structure resolved the ngEHT observing at 345 GHz [28]. M84, M104, and IC1459 are the prominent candidates on the priority list. These targets have a correlated flux density of several tens mJy [29] and a shadow size of $\sim 10 \mu\text{as}$. The sources could be directly fringed with a short solution interval and a relatively high signal-to-noise ratio at 85 GHz, that guarantees the quality of phases to be transferred to higher frequencies. The predicted sizes of black hole shadows are comparable to the resolution achievable by ngEHT at 345 GHz. It provides further test samples of black holes whether or not described by the Kerr metric besides M87* and Sgr A*. Vice versa, combining the diameter measurements of black hole shadows

with GRMHD simulations, plus an independent distance measurement, can be used to determine physical parameters of black holes (e.g., mass, orientation, and spin etc).

Towards understanding of black holes, we are still on the road of pursuing precise measurements and conclusive evidences. In the case of M84 ($z = 0.00339$, $D = 18.4$ Mpc), the mass of the central super massive black hole is $8.5 \times 10^8 M_{\odot}$ measured by the gas kinematics [30], or $1.8 \times 10^9 M_{\odot}$ estimated from velocity dispersion [31]. Therefore, the diameter d of the black hole shadow would be about $5 \mu\text{as}$ or $10 \mu\text{as}$, respectively. M84 has a correlated flux of about 80 mJy at 86 GHz (Wang et al. in press), while the baseline sensitivity of ngEHT at 86 GHz would achieve several mJy, that would guarantee the phase solutions with a signal-to-noise ratio high enough to be transferred to 345 GHz. As shown in Fig. 1, the black hole mass could be independently constrained by the angular size of the shadow. It also indicates that ngEHT with SFPR could image a batch of black hole shadows whose diameters are $\sim 10 \mu\text{as}$. SFPR could increase the coherent integration time that promises a firm fringe detection at 345 GHz, as well as high dynamic range imaging with sub-diffraction limited resolution [32].

- Detection of cosmic sources at 1mm

Based on the radio luminosity function, the number of AGNs detectable at millimeter is almost inversely proportional to the array sensitivity. Besides of detecting the horizon structure of faint nearby SMBHs, SFPR could be used to increase the detection of cosmic sources at short wavelengths. The flux threshold of SFPR detection will be ~ 10 mJy through simulations. According to the ALMA calibrator catalog¹, there would be more than nine hundred sources observable. These sources have a correlated flux (considering a resolving factor of ~ 0.16 with a baseline length of 5000 km) higher than 10 mJy and a flat spectrum from 85 GHz to 345 GHz. With the increased sensitivity of ngEHT which is further enhanced by SFPR, that provides more diverse samples approachable at the upstream of jets for physical parameter statistics, such as the brightness temperature of the mm-core and the collimation profile of the jet base [33,34], as well as sub-structures in the core region [35].

2.3. Micro-arcsecond astrometry to the black holes

SFPR enables the VLBI astrometry at millimeter/sub-millimeter wavelengths with a precision of several μas . That means 0.01 pc motions of targets can be measured within a distance of Gpc. By source-frequency phase referencing, the location of black hole could be pinpointed [29]. It enables the micro-arcsecond astrometry to the black hole itself in the ngEHT era.

¹ <https://almascience.eso.org/sc/>

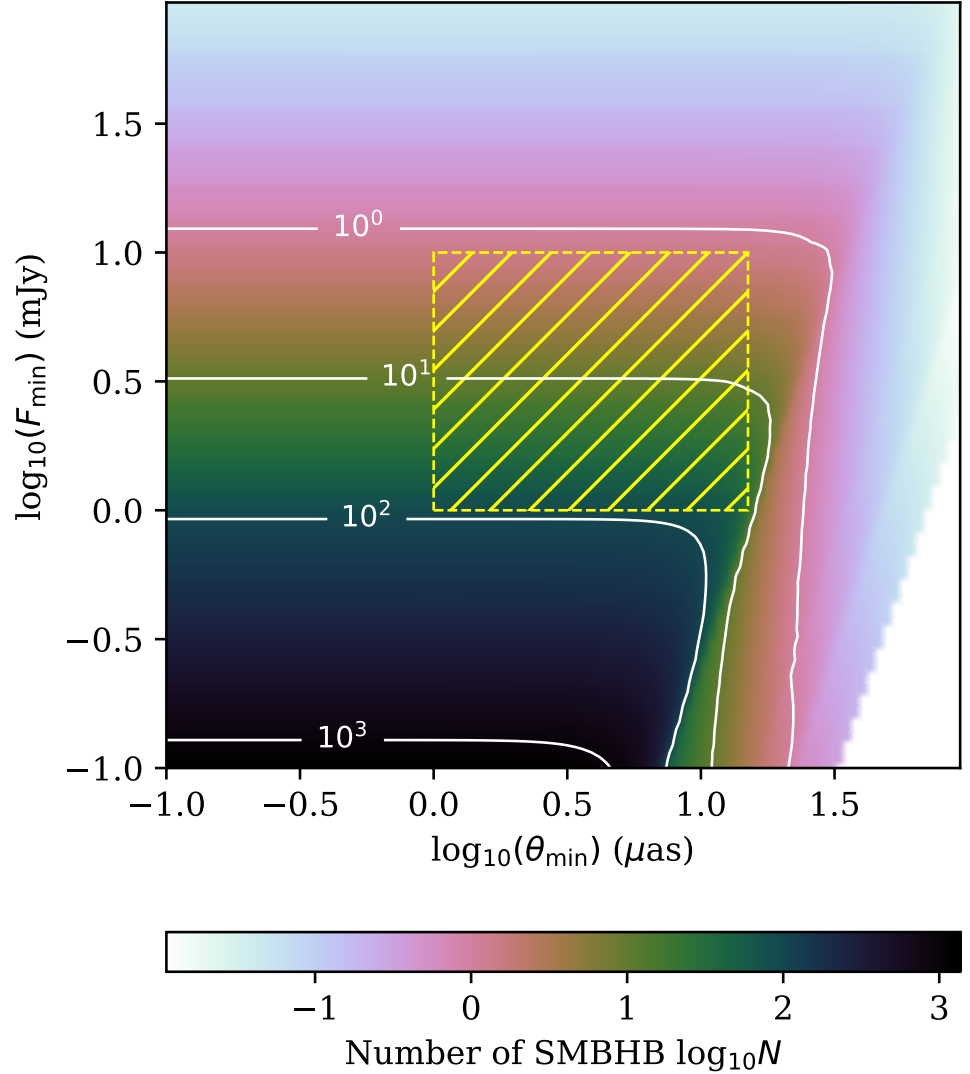


Figure 2. Number of detectable SMBHB systems (redshift $z < 0.5$) for the orbital tracking as a function of two main array parameters: the resolution θ_{\min} and the sensitivity F_{\min} . The hatched area is the target region by ngEHT, where it uses the baseline sensitivity of 10 mJy and the resolution of 15 microarcsec as the lower limit of the detection number of supermassive black hole binary systems, while the upper limit of the number is roughly corresponding to the array sensitivity and the precision of proper motion measurement by ngEHT, considering a background calibrator in the same field.

- Orbit tracking of supermassive black hole binaries

The merger of galaxies with central black holes can lead to the formation of a compact supermassive black hole binary (SMBHB) at the new galaxy center [36]. The early dynamical friction-driven and late gravitational radiation-driven phases of SMBHB evolution are separated by the sub-pc orbital separation regime. How does the SMBHB overcome this regime is known as the final-parsec problem [37]. For ngEHT with SFPR, the propagation delays caused by the troposphere could be canceled out, we can still rely on a signal-to-noise-ratio dependent resolution. Astrometric tracking of a black hole from a

SMBHB system can reach $1 \mu\text{as}$ precision or better [38,39]. In the calculation of a population of detectable SMBHBs, we adopt the fiducial parameters of the model with a larger maximum observed binary period $P_{base} = 30 \text{ yr}$ (see Table 1 in [39]), and plot the number of SMBHBs as a function of the resolution θ_{min} and the sensitivity F_{min} (Fig. 2). The ngEHT would provide an opportunity to track several observable sub-pc SMBHBs with a threshold of $\theta_{min} = 15 \mu\text{as}$ and $F_{min} = 10 \text{ mJy}$. While considering to track orbit motions of SMBHB with respect to a background source in the same field as the upper limit, the minimum threshold of θ_{min} and F_{min} is $1 \mu\text{as}$ (the static ionospheric residuals could be minimized in the in-beam scenario) and 1 mJy , respectively, as shown in Figure 2.

- **Relative and absolute astrometric measurements**

The direct astrometric output of SFPR is the core-shift. It can be the relative positions between the 85 GHz core and the photon ring of the black hole when the 340 GHz already reaches the horizon scale. Otherwise, the core-shift can be used to estimate the magnetic field and the particle density of the innermost jet [40], as well as predict the jet apex up to the infinite frequency [3]. This provides a capability to position the black hole and track its motions by synergy with the lower-frequency VLBI, where the absolute astrometry is possible. Meanwhile, the absolute astrometry at short wavelengths needs cluster/paired antennas in each site [38]. Current proper motions of SgrA* still suffer from the scattering as measured at 43 GHz [41,42], if one can go to a higher frequency, this effect can be largely reduced at the ngEHT frequencies. This is also very important to understand the head-tail sources (e.g. IC 310, NGC 1265) whose hosting galaxies are infalling into the cluster at a high speed [43].

3. Requirements

3.1. Instrumentation requirement

The capability of simultaneous observations at a lower frequency band (85 GHz or 110 GHz, 3 mm) and at one or two higher frequency bands (the 255 GHz or 220 GHz, 1.2 mm and 340 GHz or 330 GHz, 0.88 mm) is required for the frequency-phase transfer. This can be accomplished with a quasi-optics tri-band receiving system [44] or a wide band receiver [45]. In the case of a large interferometry array or co-site antennas working as single VLBI station, the capability of forming sub-arrays corresponding to the lower and the higher observing frequency bands is feasible compared to install trip-band receivers for each antenna. A co-located GPS will give accurate site positions for the geometric model, and the root-mean-square of the tropospheric path length fluctuations should be monitored for the co-site antennae. These have been found to greatly reduce the residual ionospheric, positional and tropospheric contributions. Fuller descriptions of their impact can be found in [46]. The planned recording data rate as high as 256 Gbps would be able to incorporate the multi-band data stream simultaneously since the available bandwidth will be shared across all bands. The baseline sensitivity should be high enough to guarantee the fringe detection and minimise phase errors on a correlated flux of $\sim 10 \text{ mJy}$ source at the lower frequency, as well as to achieve a super/over-resolution power [32,47]. A detailed technical demand on the instruments is presented by Rioja et al. in the same special issue.

3.2. Strategy of observation and calibration

SFPR allows a phase calibrator within 10° apart in the sky and a switching cycle of more than 10 minutes [2]. SFPR expects a calibrator of correlated flux higher enough at both the low and the high frequency bands that could be fringed. A higher flux is better as mainly to reduce the thermal noise. Meanwhile, a relative large separation, i.e., 10° makes it much less restrictive to find a suitable calibrator even at the high frequencies. The core-shift of the phase calibrator would be incorporated into the final core-shift measurement [6,48]. A prior

core-shift of calibrator or a negligible core-shift at RA or DEC direction would be helpful to extract the true core-shift of the target [7,29]. A synergy with the lower-frequency VLBI networks observing simultaneously can obtain more core-shift measurements to fit the power law scheme and perform the absolute astrometry observations.

4. Summary

With the aid of simultaneous multi-frequency receiving system and more new stations available [6,8], ngEHT with SFPR technique will be a very powerful tool to investigate the accretion disk and the jet/outflow connection in Sgr A* and M87*, or other interesting targets at sub-mm wavelengths. With dramatically increased coherence time and more feasible observational requirements (e.g. long switching cycle time and large angular separation of calibrators), it will help to capture more images of black hole shadows and detect black hole motions in a binary system or a galaxy cluster.

Acknowledgments: We thank the referees for their constructive comments and suggestions. This work was supported in part by the National Natural Science Foundation of China (grant Nos. 12173074, 11803071, 11933007), the Key Research Program of Frontier Sciences, CAS (grant Nos. QYZDJ-SSW-SLH057, ZDBS-LY-SLH011), the Shanghai Pilot Program for Basic Research - Chinese Academy of Science, Shanghai Branch (JCYJ-SHFY-2022-013), the Spanish Ministerio de Economía y Competitividad (grants AYA2016-80889-P, PID2019-108995GB-C21), the Consejería de Economía, Conocimiento, Empresas y Universidad of the Junta de Andalucía (grant P18-FR-1769), the Consejo Superior de Investigaciones Científicas (grant 2019AEP112), and the State Agency for Research of the Spanish MCIU through the "Center of Excellence Severo Ochoa" award to the Instituto de Astrofísica de Andalucía (SEV-2017-0709).

References

- Middelberg, E.; Roy, A.L.; Walker, R.C.; Falcke, H. VLBI observations of weak sources using fast frequency switching. *A&A* **2005**, *433*, 897–909, [arXiv:astro-ph/astro-ph/0412564]. <https://doi.org/10.1051/0004-6361:20042078>.
- Rioja, M.; Dodson, R. High-precision Astrometric Millimeter Very Long Baseline Interferometry Using a New Method for Atmospheric Calibration. *AJ* **2011**, *141*, 114, [arXiv:astro-ph.IM/1101.2051]. <https://doi.org/10.1088/0004-6256/141/4/114>.
- Lobanov, A.P. Ultracompact jets in active galactic nuclei. *A&A* **1998**, *330*, 79–89, [arXiv:astro-ph/astro-ph/9712132].
- Yoon, D.H.; Cho, S.H.; Yun, Y.; Choi, Y.K.; Dodson, R.; Rioja, M.; Kim, J.; Imai, H.; Kim, D.; Yang, H.; et al. Astrometrically registered maps of H₂O and SiO masers toward VX Sagittarii. *Nature Communications* **2018**, *9*, 2534, [arXiv:astro-ph.SR/1807.04455]. <https://doi.org/10.1038/s41467-018-04767-8>.
- Rioja, M.J.; Dodson, R.; Jung, T.; Sohn, B.W. The Power of Simultaneous Multifrequency Observations for mm-VLBI: Astrometry up to 130 GHz with the KVN. *AJ* **2015**, *150*, 202, [arXiv:astro-ph.IM/1509.02621]. <https://doi.org/10.1088/0004-6256/150/6/202>.
- Zhao, G.Y.; Jung, T.; Sohn, B.W.; Kino, M.; Honma, M.; Dodson, R.; Rioja, M.; Han, S.T.; Shibata, K.; Byun, D.Y.; et al. Source-Frequency Phase-Referencing Observation of AGNS with KAVA Using Simultaneous Dual-Frequency Receiving. *Journal of Korean Astronomical Society* **2019**, *52*, 23–30, [arXiv:astro-ph.IM/1903.11796]. <https://doi.org/10.5303/JKAS.2019.52.1.23>.
- Jiang, W.; Shen, Z.; Jiang, D.; Martí-Vidal, I.; Kawaguchi, N. VLBI Imaging of M81* at $\lambda = 3.4$ mm with Source-frequency Phase-referencing. *ApJL* **2018**, *853*, L14, [arXiv:astro-ph.IM/1801.04571]. <https://doi.org/10.3847/2041-8213/aaa755>.
- Rioja, M.J.; Dodson, R. Precise radio astrometry and new developments for the next-generation of instruments. *AApR* **2020**, *28*, 6, [arXiv:astro-ph.IM/2010.02156]. <https://doi.org/10.1007/s00159-020-00126-z>.
- Event Horizon Telescope Collaboration.; Akiyama, K.; Alberdi, A.; Alef, W.; Asada, K.; Azulay, R.; Baczko, A.K.; Ball, D.; Baloković, M.; Barrett, J.; et al. First M87 Event Horizon Telescope Results. I. The Shadow of the Supermassive Black Hole. *The Astrophysical Journal Letters* **2019**, *875*, L1, [1906.11238]. <https://doi.org/10.3847/2041-8213/ab0ec7>.
- Event Horizon Telescope Collaboration.; Akiyama, K.; Alberdi, A.; Alef, W.; Algaba, J.C.; Anantua, R.; Asada, K.; Azulay, R.; Bach, U.; Baczko, A.K.; et al. First Sagittarius A* Event Horizon Telescope Results. I. The Shadow of the Supermassive Black Hole in the Center of the Milky Way. *ApJL* **2022**, *930*, L12, <https://doi.org/10.3847/2041-8213/ac6674>.
- Raymond, A.W.; Palumbo, D.; Paine, S.N.; Blackburn, L.; Córdoba Rosado, R.; Doeleman, S.S.; Farah, J.R.; Johnson, M.D.; Roelofs, F.; Tilanus, R.P.J.; et al. Evaluation of New Submillimeter VLBI Sites for the Event Horizon Telescope. *ApJS* **2021**, *253*, 5, [arXiv:astro-ph.IM/2102.05482]. <https://doi.org/10.3847/1538-3881/abc3c3>.
- Doeleman, S.; Blackburn, L.; Doleman, S.; Dexter, J.; Gomez, J.L.; Johnson, M.D.; Palumbo, D.C.; Weintraub, J.; Farah, J.R.; Fish, V.; et al. Studying Black Holes on Horizon Scales with VLBI Ground Arrays. In Proceedings of the Bulletin of the American Astronomical Society, 2019, Vol. 51, p. 256.

13. Blackburn, L.; Chan, C.k.; Crew, G.B.; Fish, V.L.; Issaoun, S.; Johnson, M.D.; Wielgus, M.; Akiyama, K.; Barrett, J.; Bouman, K.L.; et al. EHT-HOPS Pipeline for Millimeter VLBI Data Reduction. *ApJ* **2019**, *882*, 23, [arXiv:astro-ph.IM/1903.08832]. <https://doi.org/10.3847/1538-4357/ab328d>.
14. Event Horizon Telescope Collaboration.; Akiyama, K.; Alberdi, A.; Alef, W.; Asada, K.; Azulay, R.; Baczko, A.K.; Ball, D.; Baloković, M.; Barrett, J.; et al. First M87 Event Horizon Telescope Results. III. Data Processing and Calibration. *ApJL* **2019**, *875*, L3, [arXiv:astro-ph.GA/1906.11240]. <https://doi.org/10.3847/2041-8213/ab0c57>.
15. Narayan, R.; Yi, I.; Mahadevan, R. Explaining the spectrum of Sagittarius A* with a model of an accreting black hole. *Nature* **1995**, *374*, 623–625. <https://doi.org/10.1038/374623a0>.
16. Yuan, F.; Quataert, E.; Narayan, R. Nonthermal Electrons in Radiatively Inefficient Accretion Flow Models of Sagittarius A*. *ApJ* **2003**, *598*, 301–312, [arXiv:astro-ph/astro-ph/0304125]. <https://doi.org/10.1086/378716>.
17. Falcke, H.; Markoff, S. The jet model for Sgr A*: Radio and X-ray spectrum. *A&A* **2000**, *362*, 113–118, [arXiv:astro-ph/astro-ph/0102186].
18. Blandford, R.D.; Königl, A. Relativistic jets as compact radio sources. *ApJ* **1979**, *232*, 34–48. <https://doi.org/10.1086/157262>.
19. Lobanov, A.P. Ultracompact jets in active galactic nuclei. *A&A* **1998**, *330*, 79–89, [arXiv:astro-ph/astro-ph/9712132].
20. Mościbrodzka, M.; Falcke, H.; Shiokawa, H.; Gammie, C.F. Observational appearance of inefficient accretion flows and jets in 3D GRMHD simulations: Application to Sagittarius A*. *A&A* **2014**, *570*, A7, [arXiv:astro-ph.HE/1408.4743]. <https://doi.org/10.1051/0004-6361/201424358>.
21. Gravity Collaboration.; Abuter, R.; Amorim, A.; Bauböck, M.; Berger, J.P.; Bonnet, H.; Brandner, W.; Clénet, Y.; Coudé Du Foresto, V.; de Zeeuw, P.T.; et al. Detection of orbital motions near the last stable circular orbit of the massive black hole Sgr A*. *A&A* **2018**, *618*, L10, [arXiv:astro-ph.GA/1810.12641]. <https://doi.org/10.1051/0004-6361/201834294>.
22. Issaoun, S.; Johnson, M.D.; Blackburn, L.; Brinkerink, C.D.; Mościbrodzka, M.; Chael, A.; Goddi, C.; Martí-Vidal, I.; Wagner, J.; Doeleman, S.S.; et al. The Size, Shape, and Scattering of Sagittarius A* at 86 GHz: First VLBI with ALMA. *ApJ* **2019**, *871*, 30, [arXiv:astro-ph.HE/1901.06226]. <https://doi.org/10.3847/1538-4357/aaf732>.
23. Cho, I.; Zhao, G.Y.; Kawashima, T.; Kino, M.; Akiyama, K.; Johnson, M.D.; Issaoun, S.; Moriyama, K.; Cheng, X.; Algaba, J.C.; et al. The Intrinsic Structure of Sagittarius A* at 1.3 cm and 7 mm. *ApJ* **2022**, *926*, 108, [arXiv:astro-ph.HE/2112.04929]. <https://doi.org/10.3847/1538-4357/ac4165>.
24. Hada, K.; Doi, A.; Kino, M.; Nagai, H.; Hagiwara, Y.; Kawaguchi, N. An origin of the radio jet in M87 at the location of the central black hole. *Nature* **2011**, *477*, 185–187. <https://doi.org/10.1038/nature10387>.
25. EHT MWL Science Working Group.; Algaba, J.C.; Anczarski, J.; Asada, K.; Baloković, M.; Chandra, S.; Cui, Y.Z.; Falcone, A.D.; Giroletti, M.; Goddi, C.; et al. Broadband Multi-wavelength Properties of M87 during the 2017 Event Horizon Telescope Campaign. *ApJL* **2021**, *911*, L11, [arXiv:astro-ph.HE/2104.06855]. <https://doi.org/10.3847/2041-8213/abef71>.
26. Blandford, R.; Meier, D.; Readhead, A. Relativistic Jets from Active Galactic Nuclei. *Annual Review of Astronomy and Astrophysics* **2019**, *57*, 467–509, [https://doi.org/10.1146/annurev-astro-081817-051948]. <https://doi.org/10.1146/annurev-astro-081817-051948>.
27. Huang, L.; Takahashi, R.; Shen, Z.Q. Testing the Accretion Flow with Plasma Wave Heating Mechanism for Sagittarius A* by the 1.3 mm VLBI Measurements. *ApJ* **2009**, *706*, 960–969, [arXiv:astro-ph.GA/0909.3687]. <https://doi.org/10.1088/0004-637X/706/2/960>.
28. Pesce, D.W.; Palumbo, D.C.M.; Narayan, R.; Blackburn, L.; Doeleman, S.S.; Johnson, M.D.; Ma, C.P.; Nagar, N.M.; Natarajan, P.; Ricarte, A. Toward Determining the Number of Observable Supermassive Black Hole Shadows. *ApJ* **2021**, *923*, 260, [arXiv:astro-ph.HE/2108.05228]. <https://doi.org/10.3847/1538-4357/ac2eb5>.
29. Jiang, W.; Shen, Z.; Martí-Vidal, I.; Wang, X.; Jiang, D.; Kawaguchi, N. Millimeter-VLBI Observations of Low-luminosity Active Galactic Nuclei with Source-frequency Phase Referencing. *ApJL* **2021**, *922*, L16, [arXiv:astro-ph.GA/2111.08930]. <https://doi.org/10.3847/2041-8213/ac375c>.
30. Walsh, J.L.; Barth, A.J.; Sarzi, M. The Supermassive Black Hole in M84 Revisited. *ApJ* **2010**, *721*, 762–776, [arXiv:astro-ph.CO/1008.0005]. <https://doi.org/10.1088/0004-637X/721/1/762>.
31. Ly, C.; Walker, R.C.; Wrobel, J.M. An Attempt to Probe the Radio Jet Collimation Regions in NGC 4278, NGC 4374 (M84), and NGC 6166. *AJ* **2004**, *127*, 119–124, [arXiv:astro-ph/astro-ph/0309743]. <https://doi.org/10.1086/379855>.
32. Akiyama, K.; Kuramochi, K.; Ikeda, S.; Fish, V.L.; Tazaki, F.; Honma, M.; Doeleman, S.S.; Broderick, A.E.; Dexter, J.; Mościbrodzka, M.; et al. Imaging the Schwarzschild-radius-scale Structure of M87 with the Event Horizon Telescope Using Sparse Modeling. *ApJ* **2017**, *838*, 1, [arXiv:astro-ph.IM/1702.07361]. <https://doi.org/10.3847/1538-4357/aa6305>.
33. Asada, K.; Nakamura, M.; Pu, H.Y. Indication of the Black Hole Powered Jet in M87 by VSOP Observations. *ApJ* **2016**, *833*, 56. <https://doi.org/10.3847/1538-4357/833/1/56>.
34. Janssen, M.; Falcke, H.; Kadler, M.; Ros, E.; Wielgus, M.; Akiyama, K.; Baloković, M.; Blackburn, L.; Bouman, K.L.; Chael, A.; et al. Event Horizon Telescope observations of the jet launching and collimation in Centaurus A. *Nature Astronomy* **2021**, *5*, 1017–1028, [arXiv:astro-ph.GA/2111.03356]. <https://doi.org/10.1038/s41550-021-01417-w>.

35. Giovannini, G.; Savolainen, T.; Orienti, M.; Nakamura, M.; Nagai, H.; Kino, M.; Giroletti, M.; Hada, K.; Bruni, G.; Kovalev, Y.Y.; et al. A wide and collimated radio jet in 3C84 on the scale of a few hundred gravitational radii. *Nature Astronomy* **2018**, *2*, 472–477, [arXiv:astro-ph.GA/1804.02198]. <https://doi.org/10.1038/s41550-018-0431-2>.
36. Kormendy, J.; Ho, L.C. Coevolution (Or Not) of Supermassive Black Holes and Host Galaxies. *ARAA* **2013**, *51*, 511–653, [arXiv:astro-ph.CO/1304.7762]. <https://doi.org/10.1146/annurev-astro-082708-101811>.
37. Begelman, M.C.; Blandford, R.D.; Rees, M.J. Massive black hole binaries in active galactic nuclei. *Nature* **1980**, *287*, 307–309. <https://doi.org/10.1038/287307a0>.
38. Broderick, A.E.; Loeb, A.; Reid, M.J. Localizing Sagittarius A* and M87 on Microarcsecond Scales with Millimeter Very Long Baseline Interferometry. *ApJ* **2011**, *735*, 57, [arXiv:astro-ph.HE/1104.3146]. <https://doi.org/10.1088/0004-637X/735/1/57>.
39. D’Orazio, D.J.; Loeb, A. Repeated Imaging of Massive Black Hole Binary Orbits with Millimeter Interferometry: Measuring Black Hole Masses and the Hubble Constant. *ApJ* **2018**, *863*, 185, [arXiv:astro-ph.HE/1712.02362]. <https://doi.org/10.3847/1538-4357/aad413>.
40. Zamaninasab, M.; Clausen-Brown, E.; Savolainen, T.; Tchekhovskoy, A. Dynamically important magnetic fields near accreting supermassive black holes. *Nature* **2014**, *510*, 126–128. <https://doi.org/10.1038/nature13399>.
41. Reid, M.J.; Brunthaler, A. The Proper Motion of Sagittarius A*. II. The Mass of Sagittarius A*. *ApJ* **2004**, *616*, 872–884, [arXiv:astro-ph/astro-ph/0408107]. <https://doi.org/10.1086/424960>.
42. Xu, S.J.; Zhang, B.; Reid, M.J.; Zheng, X.W.; Wang, G.L.; Jung, T. A Milliarcsecond Accurate Position for Sagittarius A*. *ApJ* **2022**, [arXiv:astro-ph.GA/2210.03390]. <https://doi.org/10.48550>.
43. Gendron-Marsolais, M.; Hlavacek-Larrondo, J.; van Weeren, R.J.; Rudnick, L.; Clarke, T.E.; Sebastian, B.; Mroczkowski, T.; Fabian, A.C.; Blundell, K.M.; Sheldahl, E.; et al. High-resolution VLA low radio frequency observations of the Perseus cluster: radio lobes, mini-halo, and bent-jet radio galaxies. *MNRAS* **2020**, *499*, 5791–5805, [arXiv:astro-ph.GA/2005.12298]. <https://doi.org/10.1093/mnras/staa2003>.
44. Han, S.T.; Lee, J.W.; Kang, J.; Oh, C.S.; Byun, D.Y.; Je, D.H.; Chung, M.H.; Wi, S.O.; Song, M.; Kang, Y.W.; et al. Korean VLBI Network Receiver Optics for Simultaneous Multifrequency Observation: Evaluation. *PASP* **2013**, *125*, 539. <https://doi.org/10.1086/671125>.
45. Yamasaki, Y.; Masui, S.; Ogawa, H.; Kondo, H.; Matsumoto, T.; Okawa, M.; Yokoyama, K.; Minami, T.; Konishi, R.; Kawashita, S.; et al. Development of a new wideband heterodyne receiver system for the Osaka 1.85 m mm-submm telescope: Corrugated horn and optics covering the 210–375 GHz band. *PASJ* **2021**, *73*, 1116–1127, [arXiv:astro-ph.IM/2105.13605]. <https://doi.org/10.1093/pasj/psab062>.
46. Thompson, A.R.; Moran, J.M.; Swenson, George W., J. *Interferometry and Synthesis in Radio Astronomy, 2nd Edition*; 2001.
47. Martí-Vidal, I.; Pérez-Torres, M.A.; Lobanov, A.P. Over-resolution of compact sources in interferometric observations. *A&A* **2012**, *541*, A135, [arXiv:astro-ph.IM/1203.2071]. <https://doi.org/10.1051/0004-6361/201118334>.
48. Jung, T.; Dodson, R.; Han, S.T.; Rioja, M.J.; Byun, D.Y.; Honma, M.; Stevens, J.; de Vicente, P.; Sohn, B.W. Measuring the Core Shift Effect in AGN Jets with the Extended Korean VLBI Network. *Journal of Korean Astronomical Society* **2015**, *48*, 277–284. <https://doi.org/10.5303/JKAS.2015.48.5.277>.